



Dried nanocellulose/xanthan as reinforcing fillers in thermoplastic starch

Zian Hoek · Elizabeth L. du Toit ·
Danielle Niemand · James Wesley-Smith ·
Walter W. Focke

Received: 22 November 2023 / Accepted: 4 June 2024 / Published online: 20 June 2024
© The Author(s) 2024

Abstract Nanocellulose fibres are known to enhance the mechanical properties of biopolymers when added as a filler. Nanocellulose irreversibly agglomerates upon drying and is therefore sold as an aqueous gel or suspension, increasing shipping cost and limiting application. This work studied the utility of xanthan gum as a dispersant aid for dried nanocellulose fibres. At levels as low as 15% xanthan gum addition, based on the mass of nanocellulose, prior to drying, agglomeration was significantly decreased. Mild shear rates could disperse the dried nanocellulose to a similar degree as ultrasonication when xanthan gum was present. Several complementary

techniques, such as rheology, turbidimetry, and SEM- and TEM-imaging, proved that the native nanocellulose properties could be recovered after drying. Xanthan gum and nanocellulose, when incorporated into thermoplastic starch, showed a synergistic effect regarding the increase in tensile strength of the resultant biopolymer film. The addition of previously dried nanocellulose/xanthan, in a 4:1 ratio, to thermoplastic starch at a starch-cellulose ratio of 20:1, increased the tensile strength from 5.4 to 23.0 MPa. The ability to produce a dispersible and dry nanocellulose product that retains its properties has clear commercial benefits.

Supplementary Information The online version contains supplementary material available at <https://doi.org/10.1007/s10570-024-06006-4>.

Z. Hoek · E. L. du Toit (✉) · D. Niemand · W. W. Focke
Department of Chemical Engineering, University
of Pretoria, Lynnwood Rd, Pretoria 0028, Gauteng,
South Africa
e-mail: elizbe.dutoit@up.ac.za

Z. Hoek
e-mail: zianhoek1@gmail.com

D. Niemand
e-mail: danielle1niemand@gmail.com

W. W. Focke
e-mail: walter.focke@up.ac.za

J. Wesley-Smith
EMPOWER Microscopy, Pretoria, Gauteng, South Africa
e-mail: jameswesleysmith@icloud.com

Keywords Nanocellulose · Thermoplastic starch ·
Xanthan gum · Hornification · Agglomeration

Introduction

Society has benefited from the invention of synthetic polymers, providing the world with cheap, lightweight materials that are suitable for a wide range of applications. However, the repercussions of the world's plastic consumption have come to full effect, with water and land sources being threatened by plastic pollution. The UN itself has directly stated plastic waste as a key concern in two of its sustainability development goals (United Nations 2015). Biodegradable polymers, especially those made from renewable sources, offer a possible solution.

Thermoplastic starch (TPS) is a biodegradable, renewable, and cost-effective bioplastic made from the gelatinisation of starch in the presence of a plasticiser, usually glycerol (Van Soest et al. 1996). Amura (*Tacca involucrata*) is a novel starch source originating from Nigeria (Zaku et al. 2009). It is mostly inedible, unless processed to remove toxins, and is therefore almost only consumed during famines (Janick 2024). It was investigated as a source for TPS production as it does not pose a threat to local food supply in a poverty-stricken area. That work was done in conjunction but separately with the work in this paper.

Despite the advantages, TPS has many drawbacks, such as retrogradation, high water and oxygen permeability, and especially, weak mechanical properties (Yu and Christie 2005; Mali et al. 2006; Altayan et al. 2021). Depending on the glycerol content and storage humidity, TPS has a tensile strength in the range of 2–10 MPa and a modulus ranging from 10 to 100 MPa (Zhang and Han 2006; Van Soest et al. 1996). One way to improve the mechanical properties is through filler reinforcement. Specifically, nanocellulose (NC), a high-value product derived from cellulose sourced from plant matter, bacteria, or tunicates (Foster et al. 2018), shows promise in this field. NC is not only biodegradable and renewable, but it also has a large and reactive surface area and strong mechanical properties (Dufresne 2017). NC derived from plant matter can be divided into two categories, crystalline nanocellulose (CNC), produced through acid hydrolysis (Qi et al. 2023), and cellulose nanofibre (CNF), produced via mechanical methods (Spence et al. 2011). Previous work showed that both the tensile strength and modulus of TPS doubled when reinforced with 10 wt% CNFs (Hietala et al. 2013). A significant disadvantage in the practical use of NC is the fact that it loses many of its beneficial properties upon drying.

Cellulose, when dried, undergoes hornification, the irreversible agglomeration of the cellulose fibres due to the formation of hydrogen bonds and hemiacetal bonds (lactone bridges) (Fernandes Diniz et al. 2004). It is for that reason that commercial NC contains > 75% water by mass (Foster et al. 2018). That is considerable extra mass to ship, increasing supplier cost. The water also poses an issue with hydrophobic polymers, such as polypropylene. Many solutions have been proposed to overcome this hurdle. Various drying methods, such as spray drying, freeze drying,

and super-critical drying, show promise to reduce agglomeration when compared to air- or oven-drying (Posada et al. 2020). However, all the alternative drying techniques are slower and more expensive. Surface modification, another method to prevent agglomeration, adds charged functional groups that can deter fibres from agglomerating. Examples of this are carboxymethylation or the binding of alkyl ketene dimers (Eyholzer et al. 2010; Yan et al. 2016).

The use of additives offers another possible solution (Xu et al. 2022). Some additives work through the use of ion exchange. This is usually done with oxidised NC (usually TEMPO oxidised) or NC with residual hemicelluloses (Fukuzumi et al. 2014; Yang et al. 2021). Other additives are polymers themselves, referred to as capping agents (Xu et al. 2022). It is proposed that the NC preferentially forms relatively weak bonds with the capping agent rather than bonding with other NCs. Many additives have been tested for this purpose, including carboxy methyl cellulose (CMC) (Butchosa and Zhou 2014), fish gelatin (Kwak et al. 2019), polyvinyl alcohol (PVA) (Velásquez-Cock et al. 2018), and polyethylene glycol (PEG) (Lin and Dufresne 2013). The hydrocolloid, xanthan gum, showed promise to inhibit agglomeration when it was added to TENCEL[®] gel—which are nanostructured spheres derived from cellulose Beaumont et al. (2017). Xanthan gum is commonly used as a rheology modifier in foods, with the ability to greatly increase the viscosity of suspensions (Nsengiyumva and Alexandridis 2022). It has unique chemico-physical properties, including stability over a wide pH and temperature range, 2–12 and 0–100 °C (Chaturvedi et al. 2021), respectively, and a relatively long persistence length, reported to be in the range of 100–120 nm Sato et al. (1984). Xanthan gum is also highly anionic (Chun et al. 2009). More ionic CMC was able to produce more fibrillated CNFs—confirming this as a favourable trait for a CNF capping agent Lowys et al. (2001). Its shear thinning behaviour implies that high shear mixing will ensure homogenous and effective dispersion of xanthan gum into aqueous CNF suspensions.

Despite these promising characteristics, the usefulness of xanthan gum to prevent CNF hornification has not been explored. Furthermore, there is an opacity of research on the effect of capping agents on the reinforcing ability of CNFs in biopolymer materials. This research therefore aimed to test the hypothesis

that xanthan gum can be used as an effective capping agent to produce redispersible CNFs after conventional drying. To establish whether the CNFs retain their positive effect on the mechanical properties of biopolymer materials, the resultant xanthan gum/CNFs dispersions were used to reinforce TPS films.

Experimental

Materials

Valida S191C 8% Batch SB-20-0126-01 was used as the source of CNFs, produced from hardwood, and was supplied by Sappi. The consistency (solids content) was 8.2% and the L/D ratio, as given by the supplier, was 7.08. The xanthan gum used was Ingredient Ticaxan xanthan gum 80 mesh supplied by IMCD. Amura starch was supplied by the National Root Crops Research Institute (NRCRI), Umudike in collaboration with the Raw Materials Research and Development Council (RMRDC), Abuja, Nigeria. All other chemicals used were supplied by Associated Chemical Enterprises (Acechem).

Methods

Dried CNF dispersion preparation

The CNFs were diluted to a 1 wt% concentration using deionised water after which the required amount of xanthan gum was added. The % xanthan reported is relative to the dry mass of CNFs. Mixing was achieved with a Silverson L4RT high shear mixer at 8000 rpm for 3 min. After mixing, half of the sample was retained in the non-dried state, while the other half was put in a plastic petri dish to dry in an oven at 50 °C for 24 h. The samples prepared in this manner and the associated nomenclature used are summarised in Table 1.

Mixing intensity sample preparation

The relation between the shear force applied and the force carried over to particles is shown in Eq. (1)

$$F_{\max} = 3\pi\eta\dot{\gamma}r_1r_2 \quad (1)$$

where F_{\max} is the maximum force one can apply on the particles (N), μ is the viscosity (Pa s), $\dot{\gamma}$ is the

Table 1 Nomenclature used for the various samples

Xanthan (%)	State	Group	Individual
0	Non-dried	X0	W1
	Dried		D1
15	Non-dried	X15	W2
	Dried		D2
25	Non-dried	X25	W3
	Dried		D3
50	Non-dried	X50	W4
	Dried		D4

Table 2 Mixing intensity samples nomenclature and method

Sample	Name	rpm	Time
L	Low	4000	1 min
M	Medium	5500	30 s
H	High	7000	30 s
B	Blitz	8000	30 s
U	Ultrasonic	NA	5 min

shear rate (S^{-1}), and r_1 and r_2 are the radii of the two aggregated particles (m). The formula was derived by Tadmor (1976). If the F_{\max} surpasses the intermolecular forces of the two particles, the agglomerate will break. As agglomerates are broken into smaller aggregates, the force one can apply decreases due to the decreasing particle size; thus one will reach a minimum particle size at a fixed shear rate.

Dried CNF/xanthan was diluted with deionised water to a concentration of 0.03 wt%. Table 2 describes the different mixing intensity levels applied to the samples prepared in this section with the corresponding sample names. A cumulative mixing protocol was followed. For instance, sample M was made by mixing at 4000 rpm for 1 min and then at 5500 rpm for 30 s. Sample U was therefore ultrasonicated following a sequence of all the shear mixing steps. A Jeken PS-10A ultrasonic cleaner with a frequency of 40 kHz at 70 W power was used for ultrasonication. Ultrasonication is known to be an effective albeit expensive method to disperse dried CNFs (Beck et al. 2012; Li et al. 2013). It therefore serves as a benchmark for successful sample re-dispersion when only shear mixing is applied.

TPS samples with non-dried CNF

The TPS films were made using a film casting method. Starch, 12 g, was weighed in a glass beaker. Glycerol, 30 phs (parts per hundred starch) was quickly added to prevent excessive water absorption. The required amount of CNFs and/or xanthan, non-diluted, was added. A volume of 600 mL deionized water was added and the slurry was high-shear mixed at 8000 rpm for 1 min. The samples were then heated to 85 °C within about 30 min under constant magnetic stirring. Once fully gelatinised, the samples were cast into round silicon moulds and dried overnight in a convection oven set at 50 °C. The dried films were conditioned at a relative humidity of between 53–54%, which was achieved in a chamber with a saturated $\text{Mg}(\text{NO}_3)_2$ salt solution (Greenspan 1977). The storage temperature ranged between 22–24 °C.

Xanthan gum addition resulted in persistent bubbles in the films; resistant to removal via initial degassing. Subsequently, a double casting technique was adopted due to its effective resolution of the issue. The dried films from the first casting process were blitzed into powder using a spice grinder. The powder was redissolved in 300 mL of deionised water and brought to 85 °C under constant magnetic stirring. The redissolved samples were high shear mixed once more for 1 min at 8000 rpm using a Silverson L4RT. A volume of 100 mL of deionised water was added to cool the sample. Degassing was achieved in a vacuum chamber through a step-wise decrease in pressure from 50 kPa to 40 kPa to 30 kPa. After each step change, surface bubbles were allowed to form before being scraped off. Finally, the films were recast into silicon moulds and the same drying and conditioning procedures were followed.

A face-centred central composite design (CCF) was used to estimate the linear, interaction and quadratic effects of CNFs and xanthan on the mechanical properties of TPS (Verseput 2000). The CCF design allows for the capturing of curvature as well. Two centre points were included. Note that the CNFs and xanthan quantities are in parts per hundred starch (phs). A neat TPS sample and two TPS samples with only xanthan (1.25 phs and 2.5 phs) were prepared as well. The design is shown in Table 3.

Table 3 Full CCF design with 2 centre points at 2 levels for CNFs and xanthan

No.	CNF	Xan	Level	CNF phs	Xan phs
1	−1	−1	−1	2.5	1.25
2	−1	+1	0	3.75	1.875
3	+1	−1	+1	5	2.5
4	+1	+1			
5	0	0			
6	−1	0			
7	+1	0			
8	0	−1			
9	0	+1			
10	0	0			

TPS samples with dried CNF

The TPS samples containing previously dried CNFs were prepared similarly to the ones with non-dried CNFs. The only difference is that the dried CNFs were redispersed in the deionised water at 8000 rpm for 2 min. Eight TPS samples with previously dried CNFs samples were prepared. TPS with CNF levels at low and high (−1 and +1 from Table 3), were prepared with the 4 CNF/xanthan composite samples shown in Table 1. The corresponding TPS samples with non-dried CNFs, which were not already made in the CCF design, were prepared as well.

Characterisation

FTIR

Fourier transform infrared spectroscopy (FTIR) was done on the dried CNF/xanthan composite films, as well as the pure xanthan gum powder. FTIR analysis was done using a Bruker Alpha FTIR. The scan resolution was 4 cm^{-1} and 32 scans were taken. The scan range was 7000–500 cm^{-1} . The scans were baseline corrected, smoothed, and then rescaled so that each had the same max peak height.

Zeta potential measurement

Zeta potential was measured using a Malvern Zetasizer Nano S. Both non-dried CNF/xanthan and dried CNF/xanthan were redispersed to a concentration

of 0.03 wt% in a 10 mM KNO₃ solution prepared in deionised water. The samples were redispersed via high-shear mixing. A Silverson L4RT high-shear mixer, operated at 8000 rpm for 3 min, was used for this purpose. Next, samples were ultrasonicated for 10 min to degas and further disperse the fibres. The samples were placed into DTS1070 cuvettes. Equilibration time and temperature were 3 min and 25 °C, respectively. Three sets of twelve scans were taken of each sample. Three samples of each mixture were tested.

Transmission electron microscopy (TEM)

The non-dried CNF/xanthan solutions from the zeta potential measurements were used. A drop of each sample ($\approx 5 \mu\text{L}$) was placed on one side of a Formvar-coated TEM grid. The grid was brought into contact with an equal volume of 1% aqueous phosphotungstic acid (PTA) within 15 s. The grid was immediately brought into side-on contact with filter paper to remove the excess PTA. The grid was air-dried with mild agitation. A JEOL 1010 TEM, at 100 kV, was used to image the grids. A pixel ruler, taken from RapidTable (2023), was used to estimate the fibre diameters.

Rheology

Non-dried CNF/xanthan samples, as mentioned in section “[Dried CNF dispersion preparation](#)”, were diluted by adding an equal mass of water to the non-dried sample portion. This gives a solution of ≈ 0.5 wt% CNFs. The dried CNF/xanthan samples were redispersed in deionised water to a similar concentration by shear mixing for 3 min at 8000 rpm. An Anton Paar MCR 92 rheometer with a CC 27 cup was used to measure the viscosity. Each sample was allowed to equilibrate to 25 °C for 10 min. Samples were pre-sheared at a shear rate of 50 s^{-1} for 3 s and left for a further 3 min before measurement commenced. The samples were analysed at a shear rate of $0.01\text{--}100 \text{ s}^{-1}$. Since there was shear thinning behaviour observed, the viscosity could be related to the shear rate using the power law model shown in Eq. (2)

$$\eta = K\dot{\gamma}^{n-1} \quad (2)$$

with η being the viscosity (mPa s), $\dot{\gamma}$ the shear rate (S^{-1}), and K the flow consistency index Eq. (2) can be linearised using log-transformation, shown in Eq. (3)

$$\ln \eta = \ln K + (n - 1) \ln \dot{\gamma} \quad (3)$$

The aim of the viscosity analyses was to determine whether xanthan gum allowed for more of the rheology to be retained when the CNFs are dried and redispersed. To allow quantitative comparison between the two sample types, the data sets were fitted to Eq. (4) using linear regression

$$\ln \eta = \ln K + (n - 1) \ln \dot{\gamma} + \alpha \text{ND} + \beta \ln \dot{\gamma} \text{ND} \quad (4)$$

where ND is a categorical variable that is 1 when the sample was non-dried and 0 if the sample was dried-then-redispersed. The coefficients α and β correct for the intercept and slope change between previously dried and non-dried dispersions, respectively.

Scanning electron microscopy (SEM)

Sample B (Section “[Dried CNF dispersion preparation](#)”), U (only the pure CNFs), the non-dried samples from the zeta potential measurement, and pure xanthan gum (ultrasonicated) were analysed using SEM. The samples were first freeze-dried to preserve the native suspension structure. A 1 mL aliquot of each sample was placed upon a 2×2 cm square of aluminium foil and immersed in liquid N₂. Once frozen, each foil containing the samples was transferred straight to the pre-cooled stage of a freeze dryer set at -40 °C. The freeze dryer used was a Virtis SP Scientific Advantage Pro. Samples were dried under vacuum (1.33–0.40 kPa) by slow and stepwise warming from -40 °C to room temperature over a period of two days. The dried samples were mounted on double-sided carbon adhesive dots on SEM stubs, coated with 7 nm of sputtered chromium. A Zeiss Supra55 SEM at 3 kV was used for imaging. A pixel ruler, taken from [RapidTables](#), was used to estimate the fibre diameters.

Turbidity

The mixed intensity samples, Section “[Dried CNF dispersion preparation](#)”, were used. A Cary 60

UV-Vis spectrophotometer was used to measure the absorbance. Five scans of each sample were taken due to significant variance in certain samples. Three replicates of each sample were done, except for the non-dried samples, where only 2 replicates were done. The wavelength (λ) ranged from 320 to 860 nm with a step size of 60 nm. Scan time was 2 s. The effect of xanthan was taken into account by assuming the absorbance is additive. Pure xanthan gum samples, prepared to the concentrations as in the CNF/xanthan dispersions, were scanned at each wavelength. The absorbance values for the CNF/xanthan samples were then corrected for.

Carr and Hermans (1978) derived an equation that allows the estimation of the diameter of fibrin fibres in suspension by using turbidity measurements. Turbidity here refers to the quantity, $\tau = \ln(10)A/t$, with τ being the turbidity (cm^{-1}), A the absorbance, and t the sample thickness (cm). The theory assumes that the fibrin is a thin, long rod in suspension. The scattering caused by the particles is the cause of an increase in turbidity. The turbidity can then be correlated to the particle size. Carr and Hermans (1978) made the assumption that $d \ll \lambda$, with d being the diameter (nm or cm). This assumption is not valid with larger fibres, and an alternative was proposed by Yeromonahos et al. (2010), shown in Eq. (5)

$$\tau \lambda^5 = \frac{2\pi^3}{N_A} c n' \mu \left(\frac{dn}{dc} \right)^2 \left(\frac{44}{15} \right) \left[\lambda^2 - \frac{184}{154} \pi^2 n'^2 r^2 \right] \quad (5)$$

where n' is the refractive index, dn/dc is the specific refractive index increment (mL g^{-1}), c is the concentration (g mL^{-1}), and μ is the mass-length ratio (Da cm^{-1}). A linear fit of $\tau \lambda^5$ and λ^2 allows one to estimate r and μ , with r being the fibre radius.

The shortened version of Carr-Harman's equation was used with some success on CNFs by Shimizu et al. (2016), where the μ values were determined and then related to the diameter of the fibres. The value for $\frac{dn}{dc}$ used was 0.16 mL g^{-1} , taken from Shimizu et al. (2016), and the n' used was 1.33.

Sedimentation

The mixing intensity samples in section “Dried CNF dispersion preparation” and non-dried, ultrasonicated CNF/xanthan dispersions, diluted to 0.03 wt%, were

tested. They were placed in 6 mL polytop vials. Photos were taken in 30 min time increments and quantitatively assessed to infer the degree of sedimentation with time.

Mechanical testing

The TPS films were subjected to tensile testing using an Instron 5966 universal testing system. The methodology was in accordance with the ASTM D882-18 standard. The grip separation rate was 50 mm/min with a grip separation length of 100 mm. The TPS film strip size was $16.4 \text{ mm} \times 125 \text{ mm}$. The thickness of the films was measured at three points and the average was taken. Average film thickness was $\approx 210 \mu\text{m}$. Five strips of each sample were tested. All samples tested were incubated for 10–14 d in a 54% RH chamber. The tensile values of both the neat TPS and the reinforced TPS were fitted to a quadratic formula shown in Eq. (6)

$$T = \text{CNF} + \text{Xan} + \text{CNF} \times \text{Xan} + \text{CNF}^2 + \text{Xan}^2 \quad (6)$$

where CNF and Xan refer to the CNF and xanthan levels added to the reinforced TPS. T represents either of the three tensile properties.

Results and discussion

FTIR

A comparison of the FTIR spectra of the CNF/xanthan gum composites, shown in Fig. 1, reveals a noticeable change in spectra between sample Xan15 and sample Xan25. While the spectra of Xan15 closely resemble that of pure CNFs, Xan25 shares more characteristic peaks of xanthan gum. Xanthan gum shows two distinguishable peaks at 1603 cm^{-1} and 1407 cm^{-1} . These are associated with the asymmetrical and symmetrical stretching of the COO^- groups on the xanthan sidechains, respectively (Pawlicka et al. 2019). Despite the noise in the FTIR spectra, these carboxyl peaks do seem to shift to higher wave numbers as the ratio of CNFs to xanthan increases. This alludes to possible interactions between the CNFs hydroxyl and xanthan gum carboxylate groups in the form of hydrogen bonds.

Fig. 1 FTIR spectra of dried CNFs and xanthan and their composites

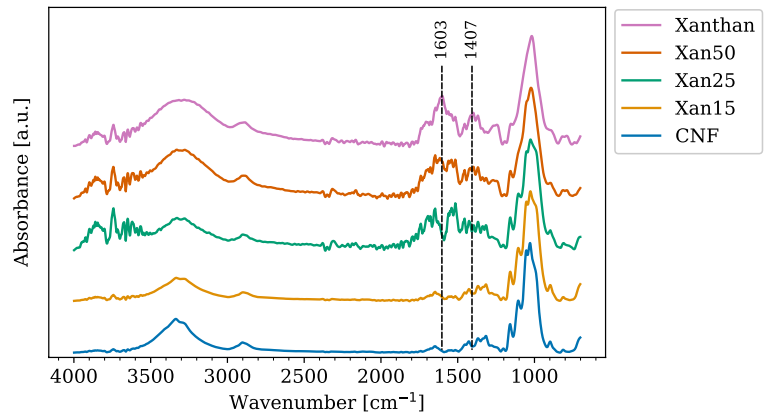


Table 4 Effect of drying and xanthan addition on the zeta potential of CNF dispersions

Dried	Xanthan (%)	Zeta potential (mV)
Yes	0	-9.9 ± 0.9
	15	-18.8 ± 1.4
	25	-22.0 ± 2.0
	50	-22.2 ± 1.3
No	0	-7.1 ± 2.5
	15	-12.8 ± 1.0
	25	-13.5 ± 1.1
	50	-18.6 ± 1.5

Colloidal stability

The zeta potential values of the CNF/xanthan gum dispersions, shown in Table 4, increase with an increase in xanthan gum content. This is to be expected since xanthan gum is anionic. Sonochemistry may explain the observed increase in the zeta potential of the samples after drying and redispersion. In this case, ultrasonication can break the hydrogen bonds and hemiacetal bonds that formed during the drying process, resulting in an increase in charged surfaces.

The images in Fig. 2 illustrate the sedimentation behaviour of CNF dispersions where xanthan gum was added at different levels prior to drying and redispersed. These solutions are compared to non-dried CNF/xanthan dispersions (Fig. 2a). The different mixing intensities applied to achieve dispersion at 0 h are also shown. It is clear that an increase in colloidal stability is achieved with the addition of xanthan gum—even for samples redispersed after drying.

This is to be expected when the increase in absolute zeta potential with an increase in xanthan gum level is considered. Pure CNFs, Fig. 2b, sediments readily when only shear mixed. Equation (1) explains the increase in dispersion stability that is achieved as the mixing intensity is increased. The smaller particle sizes predicted with an increase in shear force result in higher colloidal stability.

Subsequently, the ultrasonicated CNFs are more colloidally stable and only sediments after 24 h. The images in Fig. 2b show that shear mixing is not effective at dispersing pure, dried CNFs. The previously dried samples containing xanthan, Fig. 2c and d, show minimal sedimentation across all mixing intensities. The redispersed dried samples are more colloidally stable than their non-dried counterparts. This supports the finding of increased zeta potentials after drying. Redispersion of previously dried CNFs can thus be achieved through shear mixing when xanthan gum is used as a capping agent.

Viscosity

Table 5 shows the regression coefficients for the logarithmic transformation of the viscosity curve, Eq. (4). All curves show high linearity once logarithmically transformed ($R^2 > 0.98$). The α and β values, indicating a change in intercept and slope when compared to non-dried CNFs, are smaller for all samples where xanthan gum was added prior to drying. This proves that xanthan gum helps to preserve the native rheology of the suspension when redispersed after drying. Agglomeration of redispersed CNFs are therefore significantly inhibited through xanthan gum addition prior to drying. The p -values for all the coefficients

Fig. 2 Sedimentation results of non-dried samples (a), previously dried CNFs with no xanthan (b), with 15% xanthan (c), and with 25% xanthan (d)

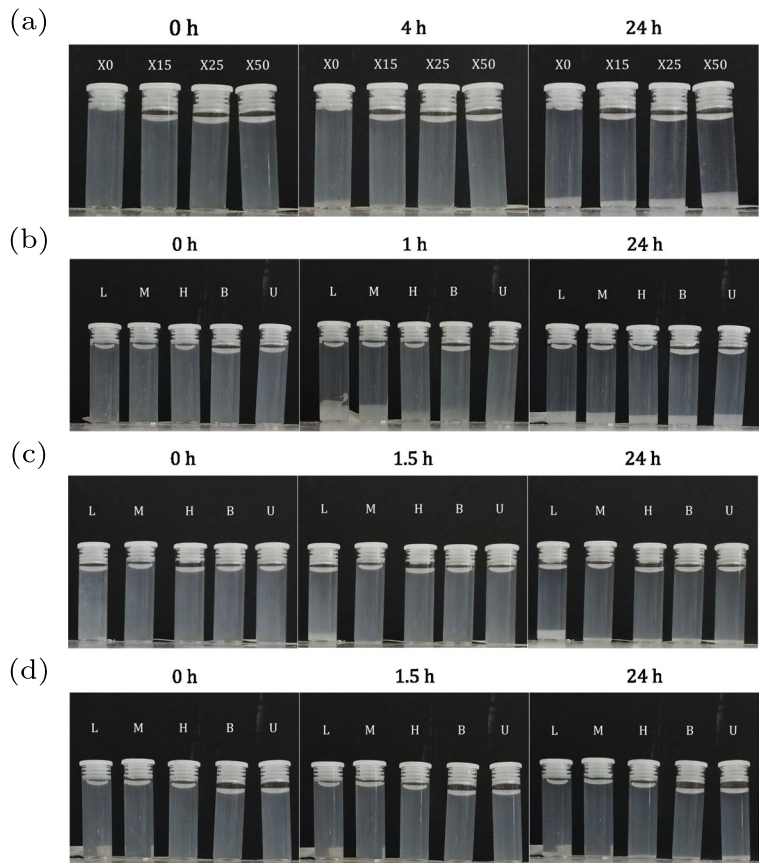


Table 5 Coefficients for a linear fit of Equation 4 to the viscosity data for the CNF/xanthan dispersions

Coeff.	Xan0	Xan15	Xan25	Xan50
$\ln K$	6.92	7.50	7.86	7.95
α	-0.42	-0.09	-0.28	-0.20
$n - 1$	-0.70	-0.75	-0.78	-0.74
β	0.06	0.00	0.03	0.02

were smaller than 0.05 except for the β -value of the Xan15 sample. This value is null within two decimal places—implying that the slopes of the logarithmically transformed X15 viscosities, both non-dried or previously dried, are indistinguishable.

TEM

The TEM images are shown in Fig. 3. A relatively high degree of agglomeration is apparent in the pure CNFs, Fig. 3a, with the CNFs bonded in a zipper-like

manner. There is a marked decrease in agglomeration with an increase in xanthan gum addition (Fig. 3b and 3c). The samples containing xanthan gum have fewer fibres glued together. This supports the hypothesis that xanthan gum can limit hornification. Using pixel measurement, the individual CNF diameter is estimated to be 10–18 nm.

SEM

The SEM images of the samples are shown in Fig. 4. Figure 4a is, as far as the authors are aware, the first image of xanthan gum in its fibrous form. It is not easy to distinguish between the CNFs and the xanthan gum, except that CNFs seem to appear coarser and xanthan more rectilinear. Figure 4b shows that ultrasonication is effective at redispersing previously dried CNFs. The fibres do seem to show some marked damage, with fibres having abrupt breakages. This may be a result of the intensity of the ultrasonication process.

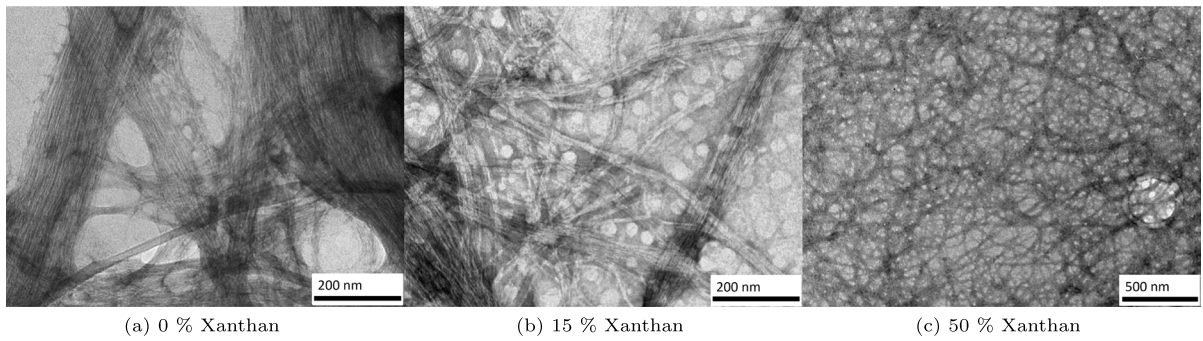
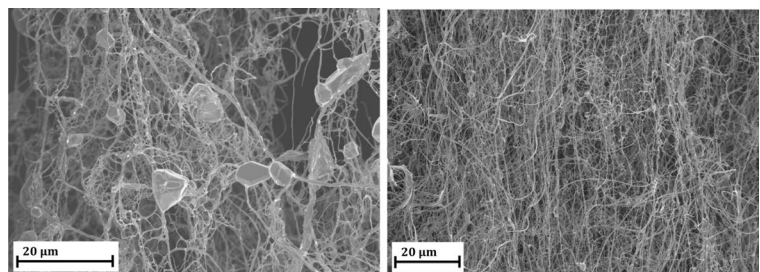


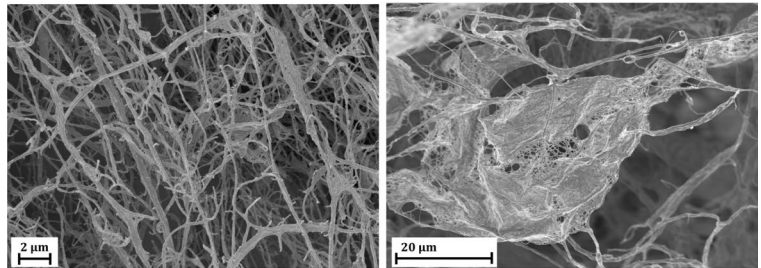
Fig. 3 TEM images of dried CNF/xanthan composites

Fig. 4 SEM images of freeze-dried CNF/xanthan suspensions

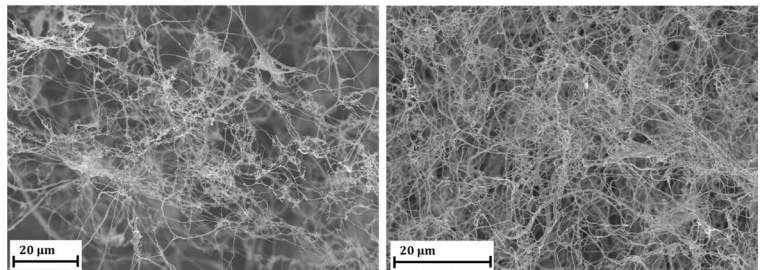


(a) Pure non-dried CNFs.

(b) Pure xanthan gum.

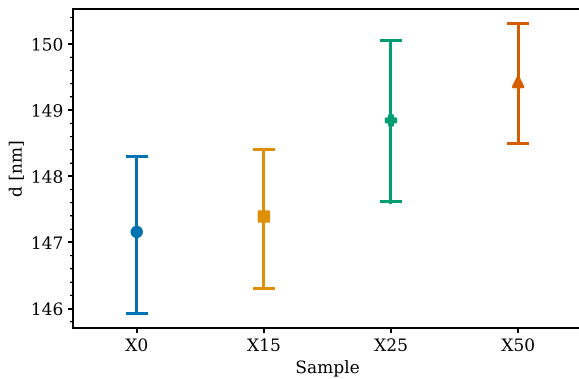


(c) Ultrasonicated, dried CNFs. (d) Shear mixed, dried CNFs.

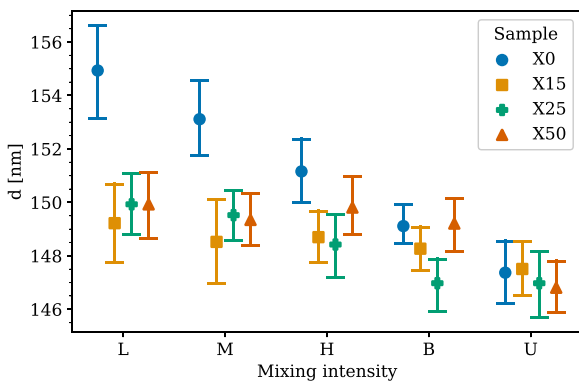


(e) Shear mixed X15 (D2) sample.

(f) Shear mixed X25 (D3) sample.



(a) Non-dried samples (ultrasonicated).



(b) Previously dried samples.

Fig. 5 Size parameters as determined by the Yeromonahos Equation, Eq. (5)

Figure 4c shows that shear mixing at 8000 rpm was ineffective at redispersing pure dried CNFs. However, at this mixing level, full redispersion is observed with the addition of 15% xanthan, and even more so with 25% xanthan (Fig. 4d and e). This provides further proof that xanthan gum is effective at producing dried CNFs that are redispersible through regular shear mixing. Using pixel measurement, the fibre diameters were estimated to be between 75–300 nm, with the majority falling in the lower range at about 125–150 nm.

Turbidimetry

The diameter estimation of CNFs using Eq. (5) is shown in Fig. 5, with the error bars indicating the 95% confidence interval. The upward drift of the

Table 6 Quadratic fit of CCF design for all tensile response variables on 30 phs glycerol TPS stored at 54% RH for 10–14 d

Coef.	Strength (MPa)	Modulus (MPa)	Elongation (%)
Intercept	$16.2 \pm 0.9^*$	$1065 \pm 97^*$	$7.8 \pm 1.1^*$
CNF	$1.7 \pm 0.7^*$	$146 \pm 66^*$	$-1.4 \pm 0.7^*$
Xan	$0.8 \pm 0.7^*$	33 ± 66	-0.5 ± 0.7
CNF:Xan	$1.0 \pm 0.8^*$	62 ± 81	0.7 ± 0.9
Xan ²	0.8 ± 1.0	76 ± 106	0.2 ± 1.2
CNF ²	0.2 ± 1.0	45 ± 106	$-1.3 \pm 1.2^*$

* p -value ≤ 0.05

estimated diameter of non-dried CNFs with increasing xanthan addition, Fig. 5a, brings into question the assumption of additive absorbance. The pure, previously dried CNF samples show a clear decrease in estimated diameter with an increase in mixing intensity (Fig. 5b). All samples containing xanthan have a near-lower limit diameter value even at the lowest mixing intensity. This implies that the intermolecular xanthan-CNF bonds are weaker than CNF-CNF bonds, allowing for easier redispersion. The X25 sample had a similar diameter (147.0 nm) at both mixing intensities B and U (p -value = 0.34). Sample X0 had diameters of 149.0 nm for B and 147.4 nm for U (p -value = 0.00). This suggests that shear mixing alone could achieve similar redispersion as ultrasonication when 25% xanthan is added but not when no xanthan is added. This supports the findings from the SEM results (Section “SEM”). The estimated diameter size of the dispersions at U mixing intensity is very similar to that of the fibres measured in the SEM Figures.

Mechanical properties

Table 6 shows the regression coefficients done on the CCF design using Eq. (6). The values in brackets indicate the 95% confidence interval. The * indicates that the coefficient is statistically significant. The tensile strength shows significance in all the linear terms, with the CNF term having the largest effect. There is a significant interaction term between CNF and xanthan. This suggests there is a synergism between the CNF and xanthan regarding tensile strength. The modulus was only influenced by the linear CNF level. The elongation was also only influenced by the CNF

Table 7 Tensile properties of 30 phs glycerol TPS stored at 54% RH for 10–14 d reinforced with non-dried or dried CNFs and xanthan at different concentrations

CNF (phs)	Xan (CNF %wt)	Non-dried			Dried		
		Strength (MPa)	Modulus (GPa)	Elongation (%)	Strength (MPa)	Modulus (GPa)	Elongation (%)
2.5	0	8.3 ± 0.5	0.44 ± 0.09	24.6 ± 2.7	10.5 ± 1.2	0.76 ± 0.08	12.2 ± 2.1
	15	9.2 ± 0.7	0.61 ± 0.07	17.0 ± 3.0	12.4 ± 0.5	0.87 ± 0.04	14.6 ± 1.5
	25	15.3 ± 0.6	1.05 ± 0.03	10.8 ± 1.5	11.8 ± 1.1	0.82 ± 0.09	13.0 ± 2.0
	50	16.3 ± 0.9	1.19 ± 0.11	7.7 ± 1.6	14.3 ± 1.1	1.01 ± 0.13	9.4 ± 1.4
5	0	14.3 ± 2.9	1.04 ± 0.32	9.1 ± 2.1	15.3 ± 1.0	1.03 ± 0.06	11.0 ± 1.7
	15	12.9 ± 1.7	0.94 ± 0.18	14.3 ± 2.5	19.4 ± 2.1	1.31 ± 0.16	9.5 ± 2.3
	25	17.0 ± 0.7	1.25 ± 0.08	4.7 ± 0.9	23.0 ± 0.7	1.48 ± 0.07	7.0 ± 0.8
	50	20.9 ± 1.7	1.42 ± 0.11	6.3 ± 0.8	19.4 ± 1.3	1.46 ± 0.15	7.9 ± 0.7

level but both linearly and quadratically. The quadratic and linear CNF coefficients for elongation are also similar, suggesting that there is a plateau at low loadings of CNF and that there is a sharp increase as the CNF loading gets higher. This suggests that at a certain loading, one can achieve a continuous CNF phase throughout the TPS matrix. The theory is that, if there are discontinuous phases, they can not work as one cohesive unit to reinforce the polymer, meaning that elongation can still occur in certain parts of the TPS as if the CNFs was not there.

The pure TPS has an average tensile strength, modulus and elongation of 5.4 MPa, 0.31 GPa, and 56.4%, respectively. With 1.25 phs xanthan added (absent of CNFs), the tensile strength is 6.5 MPa, modulus 0.16 GPa, and elongation 46.9%. This is not much different from the pure TPS sample. TPS with 2.5 phs xanthan addition exhibits an average tensile strength, modulus and elongation of 9.6 MPa, 0.61 GPa, and 19.9%, respectively. This is a marked change. The shift in tensile properties from 1.25 phs xanthan to 2.5 phs xanthan can be explained by the formation of a continuous network. If this is true, there is a critical concentration where xanthan gum forms a continuous phase through the polymer matrix, allowing it to be fully reinforced.

The tensile results of TPS reinforced with CNF/xanthan composites, both non-dried and dried-then-redispersed, are shown in Table 7. There is no conclusive difference between the TPS with non-dried CNF/xanthan and TPS with previously dried CNF/xanthan. It is suggested that the high compatibility between TPS and CNFs makes it an inadequate polymer to

test the influence of agglomeration on the tensile properties. There are nonetheless noteworthy observations. There is a marked decrease in elongation at the 2.5 phs CNF TPS samples when 50% xanthan, relative to the mass CNFs, is added. This supports the theory that there is a continuous network that forms once one has enough filler in the polymer matrix. The best result achieved was the dried 5 phs CNF sample with 25% xanthan, which showed a tensile strength of 23.0 MPa and a modulus of 1.48 GPa.

Conclusion

This study demonstrates that the addition of xanthan gum produces dried CNFs that can be redispersed with shear mixing alone. The shear thinning behaviour of non-dried and previously dried pure CNF suspensions differs significantly. The addition of 15% xanthan gum eliminates the difference in shear-thinning slopes. Turbidity analyses indicate that higher mixing intensities and xanthan gum addition produce more dispersed CNF suspensions. Shear mixing alone can not fully redisperse pure, dried CNFs, but CNFs with 25% xanthan gum is just as dispersed with shear mixing as with ultrasonication. SEM imaging confirms these findings, showing that ultrasonication is necessary to redisperse pure, dried CNFs. However, CNF/xanthan dispersions, whether previously dried and shear mixed or non-dried and ultrasonicated, appear identical.

The study also demonstrates the interaction between xanthan and CNFs as reinforcing fillers in

TPS. Quadratic regression of the tensile strength results reveals a significant positive interaction between CNFs and xanthan gum. No clear difference is observed between TPS reinforced with previously dried or non-dried CNF/xanthan dispersions, even in the absence of xanthan gum, and this is probably due to the high compatibility between cellulose and starch. The highest tensile strength (23.0 MPa) and modulus (1.48 GPa) are achieved in TPS reinforced with previously dried 5 phs CNFs containing 25% xanthan, relative to the CNFs.

The findings prove that xanthan gum is effective at producing fully redispersible CNFs and does not subtract from the reinforcing qualities of CNFs in TPS but rather enhances it. Future research should investigate the use of dried CNF/xanthan gum in polymers less compatible with cellulose, such as polylactic acid. This research contributes to the use of nanocellulose as a polymer additive.

Acknowledgements The authors also thank Sappi for supplying the nanocellulose fibre samples and assisting with the rheological characterisation of the samples.

Author contributions Zian Hoek prepared all the figures James Wesley-Smith did SEM and TEM analysis Zian Hoek and Danielle Niemand did all other experimental work All authors contributed to the analysis of the data Zian Hoek and Elizabeth L. du Toit wrote the manuscript text All authors reviewed the manuscript

Funding Open access funding provided by University of Pretoria. Financial support from Paper Manufacturers Association of South Africa (PAMSA) and the Department of Science and Innovation under Grant No. DST/CON 0004/2019 is gratefully acknowledged.

Availability of data and materials The data that support the findings of this study are available in the University of Pretoria's data repository (Hoek 2023), and contain the values for the tensile results, turbidity, and viscosity measurements. Data-sets are also uploaded as supporting information.

Declarations

Competing interest The authors have no competing interest to declare.

Ethical approval Not applicable.

Open Access This article is licensed under a Creative Commons Attribution 4.0 International License, which permits use, sharing, adaptation, distribution and reproduction in any

medium or format, as long as you give appropriate credit to the original author(s) and the source, provide a link to the Creative Commons licence, and indicate if changes were made. The images or other third party material in this article are included in the article's Creative Commons licence, unless indicated otherwise in a credit line to the material. If material is not included in the article's Creative Commons licence and your intended use is not permitted by statutory regulation or exceeds the permitted use, you will need to obtain permission directly from the copyright holder. To view a copy of this licence, visit <http://creativecommons.org/licenses/by/4.0/>.

References

- Altayan MM, Darouich TA, Karabet F (2021) Thermoplastic starch from corn and wheat: a comparative study based on amylose content. *Polym Bull* 78:3131–3147. <https://doi.org/10.1007/S00289-020-03262-9>
- Beaumont M, König J, Opietnik M, Potthast A, Rosenau T (2017) Drying of a cellulose II gel: effect of physical modification and redispersibility in water. *Cellulose* 24:1199–1209. <https://doi.org/10.1007/s10570-016-1166-9>
- Beck S, Bouchard J, Berry R (2012) Dispersibility in water of dried nanocrystalline cellulose. *Biomacromolecules* 13:1486–1494. <https://doi.org/10.1021/BM300191K>
- Butchosa N, Zhou Q (2014) Water redispersible cellulose nanofibrils adsorbed with carboxymethyl cellulose. *Cellulose* 21:4349–4358. <https://doi.org/10.1007/s10570-014-0452-7>
- Carr ME, Hermans J (1978) Size and density of fibrin fibers from turbidity. *Macromolecules* 11:46–50. <https://doi.org/10.1021/ma60061a009>
- Chaturvedi S, Kulshrestha S, Bhardwaj K, Jangir R (2021) *Microbial Polymers* (Springer), chap. A Review on Properties and Applications of Xanthan Gum, pp 87–107. https://doi.org/10.1007/978-981-16-0045-6_4
- Chun MS, Kim C, Lee DE (2009) Conformation and translational diffusion of a xanthan polyelectrolyte chain: Brownian dynamics simulation and single molecule tracking. *Phys Rev* 79:051919. <https://doi.org/10.1103/PhysRevE.79.051919>
- Dufresne A (2017) Cellulose nanomaterial reinforced polymer nanocomposites. *Curr Opin Colloid Interface Sci* 29:1–8. <https://doi.org/10.1016/j.cocis.2017.01.004>
- Eyholzer C, Bordeanu N, Lopez-Suevos F, Rentsch D, Zimmermann T, Oksman K (2010) Preparation and characterization of water-redispersible nanofibrillated cellulose in powder form. *Cellulose* 17:19–30. <https://doi.org/10.1007/S10570-009-9372-3>
- Fernandes Diniz JMB, Gil MH, Castro JAAM (2004) Hornification—its origin and interpretation in wood pulps. *Wood Sci Technol* 37:489–494. <https://doi.org/10.1007/s00226-003-0216-2>
- Foster EJ, Moon RJ, Agarwal UP, Bortner MJ, Bras J, Camarero-Espinosa S, Chan KJ, Clift MJD, Cranston ED, Eichhorn SJ, Fox DM, Hamad WY, Heux L, Jean B, Korey M, Nieh W, Ong KJ, Reid MS, Renneckar S, Roberts R, Shatkin JA, Simonsen J, Stinson-Bagby K, Wanasekara

- N, Youngblood J (2018) Current characterization methods for cellulose nanomaterials. *Chem Soc Rev* 47:2609–2679. <https://doi.org/10.1039/c6cs00895j>
- Fukuzumi H, Tanaka R, Saito T, Isogai A (2014) Dispersion stability and aggregation behavior of tempo-oxidized cellulose nanofibrils in water as a function of salt addition. *Cellulose* 21:1553–1559. <https://doi.org/10.1007/s10570-014-0180-z>
- Greenspan L (1977) Humidity fixed points of binary saturated aqueous solutions. *J Res Natl Bur Stand A Phys Chem* 81(1):89–96
- Hietala M, Mathew AP, Oksman K (2013) Bionanocomposites of thermoplastic starch and cellulose nanofibers manufactured using twin-screw extrusion. *Eur Polym J* 49:950–956. <https://doi.org/10.1016/J.EURPOLYMJ.2012.10.016>
- Hoek Z (2023) Rheology, turbidity and tensile data for nanocellulose and xanthan composites. <https://doi.org/10.25403/UPresearchdata.24265162>
- Janick J, Freedman B (2024) *Tacca involucreta*. https://www.purdue.edu/hla/sites/famine-foods/famine_food/tacca-involucreta/
- Kwak HW, You J, Lee ME, Jin HJ (2019) Prevention of cellulose nanofibril agglomeration during dehydration and enhancement of redispersibility by hydrophilic gelatin. *Cellulose* 26:4357–4369. <https://doi.org/10.1007/S10570-019-02387-Z>
- Lin N, Dufresne A (2013) Physical and/or chemical compatibilization of extruded cellulose nanocrystal reinforced polystyrene nanocomposites. *Macromolecules* 46:5570–5583. <https://doi.org/10.1021/MA4010154>
- Li Q, McGinnis S, Sydnor C, Wong A, Renneckar S (2013) Nanocellulose life cycle assessment. *ACS Sustain Chem Eng* 1:919–928. <https://doi.org/10.1021/sc4000225>
- Lowys MP, Desbrières J, Rinaudo M (2001) Rheological characterization of cellulosic microfibril suspensions. role of polymeric additives. *Food Hydrocoll* 15:25–32. [https://doi.org/10.1016/S0268-005X\(00\)00046-1](https://doi.org/10.1016/S0268-005X(00)00046-1)
- Mali S, Grossmann MVE, García MA, Martino MN, Zaritzky NE (2006) Effects of controlled storage on thermal, mechanical and barrier properties of plasticized films from different starch sources. *J Food Eng* 75(4):453–460. <https://doi.org/10.1016/j.jfoodeng.2005.04.031>
- Nsengiyumva EM, Alexandridis P (2022) Xanthan gum in aqueous solutions: fundamentals and applications. *Int J Bio Macromol* 216:583–604. <https://doi.org/10.1016/J.IJBIOMAC.2022.06.189>
- Pawlicka A, Tavares FC, Dörr DS, Cholant CM, Ely F, Santos MJL, Avellaneda CO (2019) Dielectric behavior and ftir studies of xanthan gum-based solid polymer electrolytes. *Electrochim Acta* 305:232–239. <https://doi.org/10.1016/J.ELECTACTA.2019.03.055>
- Posada P, Velásquez-Cock J, Gómez-Hoyos C, Serpa Guerra AM, Lyulin SV, Kenny JM, Gañán P, Castro C, Zuluaga R (2020) Drying and redispersion of plant cellulose nanofibers for industrial applications: a review. *Cellulose* 27:10649–10670. <https://doi.org/10.1007/S10570-020-03348-7>
- Qi Y, Guo Y, Liza AA, Yang G, Sipponen MH, Guo J, Li H (2023) Nanocellulose: a review on preparation routes and applications in functional materials. *Cellulose* 30:4115–4147. <https://doi.org/10.1007/s10570-023-05169-w>
- RapidTable (2023). <https://www.rapidtables.com/web/tools/pxel-ruler.html>. Visited on 2023-10-23
- Sato T, Norisuye T, Fujita H (1984) Double-stranded helix of xanthan: Dimensional and hydrodynamic properties in 0.1 M aqueous sodium chloride. *Macromolecules* 17:2696–2700. <https://doi.org/10.1021/ma00142a043>
- Shimizu M, Saito T, Nishiyama Y, Iwamoto S, Yano H, Isogai A, Endo T (2016) Fast and robust nanocellulose width estimation using turbidimetry. *Macromol Rapid Commun* 37:1581–1586. <https://doi.org/10.1002/MARC.201600357>
- Spence KL, Venditti RA, Rojas OJ, Habibi Y, Pawlak JJ (2011) A comparative study of energy consumption and physical properties of microfibrillated cellulose produced by different processing methods. *Cellulose* 18:1097–1111. <https://doi.org/10.1007/s10570-011-9533-z>
- Tadmor Z (1976) Forces in dispersive mixing. *Ind Eng Chem Fundam* 15:346–348. <https://doi.org/10.1021/1160060A022>
- United Nations. Transforming our world: The 2030 agenda for sustainable development (2015). <https://wedocs.unep.org/20.500.11822/9814>
- Van Soest JGG, Bezemer RC, de Wit D, Vliegthart JFG (1996) Influence of glycerol on the melting of potato starch. *Ind Crops Prod* 5:1–9. [https://doi.org/10.1016/0926-6690\(95\)00047-X](https://doi.org/10.1016/0926-6690(95)00047-X)
- Van Soest JGG, Hulleman SHD, de Wit D, Vliegthart JFG (1996) Changes in the mechanical properties of thermoplastic potato starch in relation with changes in b-type crystallinity. *Carbohydr Polym* 29:225–232. [https://doi.org/10.1016/0144-8617\(96\)00011-2](https://doi.org/10.1016/0144-8617(96)00011-2)
- Velásquez-Cock J, Gómez H BE, Posada P, G AS, Gómez H C, Castro C, Gañán P, Zuluaga R (2018) Poly (vinyl alcohol) as a capping agent in oven dried cellulose nanofibrils. *Carbohydr Polym* 179:118–125. <https://doi.org/10.1016/J.CARBPOL.2017.09.089>
- Verseput R (2000) Digging into doe: Selecting the right central composite design for response surface methodology applications. *Quality Digest*. <https://www.qualitydigest.com/june01/html/doe.html>
- Xu Y, Xu Y, Chen H, Gao M, Yue X, Ni Y (2022) Redispersion of dried plant nanocellulose: a review. *Carbohydr Polym* 294:119830. <https://doi.org/10.1016/J.CARBPOL.2022.119830>
- Yang G, Ma G, He M, Ji X, Li W, Youn HJ, Lee HL, Chen J (2021) Comparison of effects of sodium chloride and potassium chloride on spray drying and redispersion of cellulose nanofibrils suspension. *Nanomaterials* 11:439. <https://doi.org/10.3390/NANO11020439>
- Yan Y, Amer H, Rosenau T, Zollfrank C, Dörrstein J, Jobst C, Zimmermann T, Keckes J, Veigel S, Gindl-Altmatter W, Li J (2016) Dry, hydrophobic microfibrillated cellulose powder obtained in a simple procedure using alkyl ketene dimer. *Cellulose* 23:1189–1197. <https://doi.org/10.1007/s10570-016-0887-0>
- Yeromonahos C, Polack B, Caton F (2010) Nanostructure of the fibrin clot. *Biophys J* 99:2018–2027. <https://doi.org/10.1016/J.BPJ.2010.04.059>
- Yu L, Christie G (2005) Microstructure and mechanical properties of orientated thermoplastic starches. *J Mater Sci* 4:111–116. <https://doi.org/10.1007/S10853-005-5694-1>

- Zaku S, Aguzue O, Thomas S, Barminas J (2009) Studies on the functional properties and the nutritive values of amara plant starch (*Tacca involucrata*) a wild tropical plant. *Afr J Food Sci* 3(10):320–322
- Zhang Y, Han JH (2006) Mechanical and thermal characteristics of pea starch films plasticized with monosaccharides and polyols. *J Food Sci* 71(2):109–118. <https://doi.org/10.1111/j.1365-2621.2006.tb08891.x>

Publisher's Note Springer Nature remains neutral with regard to jurisdictional claims in published maps and institutional affiliations.